

**MEASUREMENTS OF OCEAN SURFACE STRESS
USING AIRCRAFT SCATTEROMETERS**

**David E. Weissman
Dept. of Engineering
Hofstra University
Hempstead, New York 11550**

**Fuk K. Li, Shu-hsiang Lou, Son V. Nghiem and Gregory Neumann
Jet Propulsion Laboratory
California Institute of Technology
California, Pasadena, CA 91109**

**Robert E. McIntosh, Steven C. Carson and James R. Carswell
Department of Electrical Engineering
University of Massachusetts
Amherst, MA 01003**

**Hans C. Graber
Rosenstiel School of Marine and Atmospheric Sciences
University of Miami
Miami, Florida 33149-1098**

**Robert E. Jensen
Coastal Engineering Research Center
U.S. Army Corps of Engineers
Vicksburg, MS 39180-6199**

Submitted to: Journal of Atmospheric and Oceanic Technology

January 1996

ABSTRACT

Scatterometer model functions which directly estimate friction velocity, have been developed and are being tested with radar and in-situ data acquired during the Surface Wave Dynamics Experiment of 1991. Both KU-band and C-band scatterometers were operated simultaneously for extensive intervals for each of 10 days during SWADE. The model function developed previously from the FASINEX experiment converts the KU-band RCS measurements into friction velocity estimates. These are compared to in-situ, estimates of surface wind stress and direction across a wide area both on and off the Gulf Stream (for hourly intervals), which were determined from buoy and meteorological measurements during February and March, 1991. The Ku-band estimates of u_* magnitude are in excellent agreement with the in-situ values. The C-Band scatterometer measurements were coincident with the Ku-band RCS, whose u_* estimates are then used to calibrate the C-band. The results show the C-band RCS dependence at 20,30, 40 and 50 degrees to be less sensitive to friction velocity than the corresponding cases for Ku-band. The goal is to develop the capability of making friction velocity estimates (and surface stress) from radar cross section data acquired by satellite scatterometers.

1.. INTRODUCTION

The long term goal of this research is to provide direct estimates of global sea surface wind stress, derived from satellite scatterometer observations. These radar cross section observations will be utilized by new, empirically derived model functions based on the relationship between normalized radar cross section (NRCS) and friction velocity at the surface. The model functions (Ku-band for NSCAT and C-band for ERS-1 and ERS-2) for friction velocity described below were derived from major, large scale field experiments in which airborne scatterometers collected data over a wide range of oceanic and atmospheric conditions, while coincident in-situ observations were also made. The results presented in this paper illustrate the performance and potential accuracy of these model functions using independent estimates of u' for this evaluation. This will be of strong interest to the oceanographic community involved in the utilization of satellite remote sensing data to study circulation and currents with models driven by wind forcing.

It has been about 20 years since the SEASAT-A scatterometer first provided global surface wind estimates. These were based on algorithms calibrated with wind speed data, and were intended to provide wind vectors, not stress estimates. In the interim, there have been numerous expressions from members of the remote sensing community calling for direct estimates of friction velocity and stress using algorithms specifically developed for this purpose. [O'Brien, 1982]. Official publications of the NSCAT [Freilich, 1980] and WOCE [Freilich, 1995] projects indicate that wind stress is one of the required measurements. Another related, and fundamental issue, is that the FASINEX data analysis indicates a more direct physical relationship between the radar cross section and

friction velocity, then with wind speed in many situations (at a particular reference height). When the applications of these satellite-derived winds require their conversion to stress using a drag coefficient (either a simple constant, or with an additional wind variable) then errors, caused by the actual variability of the drag coefficient, are likely to occur,

The major missions of the NSCAT project and the ERS scatterometer project to develop global scale wind estimates as their continuous data product are well organized and in progress. However there has never been a comparable effort to develop and implement a similar model function for surface stress. Therefore, the usual practice in applications which require stress estimates is to convert the satellite wind estimates, coupled with a drag coefficient estimate, into a stress quantity. While it has been known for some time how the drag coefficient depends on speed [Smith, 1988; Anderson, 1993], numerous recent studies have also shown how important the influence of sea state, wave age and mixed sea conditions are to the magnitude of the drag coefficient [Geernaert, 1990; Nordeng, 1991; Smith, et al, 1992; and Donelan, et al, 1993], None of this knowledge can be utilized with a wind speed estimate because the satellite scatterometers do not have any means of independently obtaining coincident sea state, swell or spectrum information that could be used to support an algorithm for a multi-variable drag coefficient. Of course a friction velocity model function can go to the heart of the matter, since the drag coefficient dependencies are built-in during its creation.

Part of the motivation for conducting airborne radar scatterometer field measurements during FASINEX and SWADE was to create a data base for the development of a friction

velocity algorithm, This effort began in the mid-1 980's in response to the "Report of the Satellite Stress Working Group" [O'Brien, et al, 1982]. It was vigorously noted then that "...ocean surface wind stress measurements are needed to drive ocean circulation models". In the interim, no satisfactory techniques have been found that estimate the stress from radar cross section measurement. There have been no other aircraft scatterometer flight programs that have gathered any meaningful stress measurements for empirical algorithm development, to the best of the authors' knowledge, beyond those mentioned here.

There are several examples in the literature of studies concerned with utilizing satellite wind estimates from ERS-1 and/or NSCAT simulations. The simulations by Barnier, Boukthir and Verron [1991] and Barnier, Capella and O'Brien [1 994] depend on estimates of sea surface stress. The only recourse they have is to start with wind estimates and then assume a constant drag coefficient across wide expanses of the ocean, The study of the Indian Ocean and tropical Pacific using actual ERS-1 wind estimates by Legler and O'Brien [1993] leaves some discrepancies between the predictions of their ocean model and sea level data, A recent study by Caruso, et al [1994b] used ERS-1 wind forcing to study the California, North Equatorial and Kuroshio currents, with mixed results, An important common issue in all of these instances is how to distinguish between the differences caused by deficiencies of a particular ocean model and those resulting from having to use wind estimates from the satellite sensors, instead of direct the wind stress values,

2. BACKGROUND

a. FASINEX

The Frontal Air-Sea Interaction Experiment (FASINEX) was a cooperative program to investigate the role of horizontal variability in air-sea interaction in the vicinity of a sea surface temperature front. It took place during the Winter- Spring of 1985-86. [Stage & Weller, 1985; Stage & Weller, 1986] There was coincident airborne Scatterometer measurements of the ocean surface radar cross section at K-band with wind speed and wind stress measured close to the surface,

The NASA-JPL Ku-band Scatterometer data was obtained from 10 measurement flights during FASINEX. A total of approximately 30 hours of data were collected, under a wide range of sea and environmental conditions [Li, et al, 1989]. Winds encountered ranged from 2 to 20 m/s. Stress measurements were inferred from ship-board instruments and from aircraft flying at low altitudes, closely following the scatterometer.

These data have been analyzed to study separate, new model functions for both wind speed and surface friction velocity (square root of kinematic wind stress), and to better understand the physics of the air-sea interaction across a variety of spatial scales. These studies indicate that the surface stress has a more direct and consistent influence on the radar cross section than does the neutral wind speed. The difference between the NRCS models using these two variables depends on the polarization and the incidence angle. In most cases the advantage gained by using the friction velocity model function to estimate the surface quantity is substantial, in a few others it is small [Weissman, et al, 1994],

b. SWADE

The Surface Wave Dynamics Experiment took place off the east coast of the United States in the region 35°N to 42°N and 70°W to 76°W during the period from October 1990 to March 1991. The objectives of SWADE include the direct measurement of wind stress, sensible and latent heat fluxes, in conjunction with detailed measurements of the sea state, for analysis of the relationship between variability in the fluxes and sea state [Weller, et al., 1991]. It is precisely this variability in the momentum flux, related to the long wave sea state, that will affect the small scale roughness (which controls the microwave radar cross section) of the surface in a manner that can best be perceived with a friction velocity model function.

The aircraft scatterometer measurements during SWADE took place between Feb. 27 and March 9, 1991, during the 3rd Intensive Observation Period (IOP-3) of the entire project. The principle experiment area was east of the Virginia coast, in the vicinity of NOAA-NDBO, CERC and other buoys (near 74 deg. West Long., and 37 deg. Lat) [Caruso, et al, 1993, Caruso, et al, 1994]. Numerous flight lines crossed the Gulf Stream boundary [Nghiem, et al, 1995]

The KU-band radar (operating at 14 GHz) [Nghiem, et al., 1995] and the C-band (5 GHz, V-pol) radar were mounted for simultaneous and co-located observations, on a NASA C-130B aircraft, [McLaughlin, et al, 1991; Carson, 1992, Carswell, et al, 1995]. Both antennas rotated azimuthally in a nearly complete circle at each selected incidence angle, with most data between 20 and 50 degrees incidence angle,

During flight segments where the aircraft follows a straight path typically 50 to 100 km long, the usual scan interval for one cycle of antenna rotation lasts 2 to 3 minutes, for a fixed set of radar parameters, This corresponded to one revolution for the KU-band antenna, During this cycle time the aircraft moves 14 to 20 km. The C-band antenna rotation rate is 20 rpm resulting in multiple looks at each azimuth angle. Successive flight line segments may be averaged together.

C-Band (5 GHz) scatterometer measurements were combined with coincident sea surface friction velocity estimates to create a new model function. The goal is to develop a model function for C-band with the capability of making friction velocity estimates (and surface stress) from radar cross section data acquired by the ERS-1 satellite scatterometer.

Both Ku-band and C-band scatterometers were operated simultaneously for extensive intervals for each of 10 days during SWADE. The model function that was developed previously from the FASINEX experiment converts the KU-band RCS measurements into friction velocity. These estimates of friction velocity then serve as the coincident surface measurements for the C-band system The results to be presented will show the C-band RCS dependence at 20,30, 40 and 50 degrees to be less sensitive to friction velocity than the corresponding cases for Ku-band, The analysis of these radar data is providing results which are suitable for the development of a full algorithm for C-band (for all incidence and azimuthal angles) [Weissman,1994]; Davidson, et al,1995]

Spatial variations of u_* across the Gulf Stream derived from the Ku-band radar data

are studied in conjunction with supporting measurements of air-sea temperature, wind and wave fields. These u estimates were then compared with the approximately coincident and concurrent friction velocity estimates derived from the SWADE wave hindcast model prediction of IOP-3 (Caruso et al. 1994). They were updated every hour and spanned the entire SWADE region of interest, The SWADE buoys provide both physical oceanographic and meteorological data at points within the flight pattern. Wind conditions surveyed in this study ranged from 5 to 12 m/s. A detailed discussion of the analysis of the in-situ measurements and related data appears in the following section. This comparison between the radar and in-situ estimates of u is 'serving as an independent test of the Ku-band FASINEX algorithm.

3. IN-SITU MEASUREMENTS, ANALYSIS AND PREDICTIONS

Six alternative wind fields were originally employed in the analysis of SWADE IOP-3 discussed in Caruso et al. (1994). However, for this study we used the results from the wave simulation forced by the wind field of Oceanweather, Inc. (OWI). This wind field was derived by intensive manual kinematic reanalysis using all conventional and special SWADE meteorological data. Details of the wind field reanalysis procedures and methodologies is described in Cardone et al. (1995), The intent of the OWI analysis is to resolve the "synoptic scale" wind field at three-hourly intervals on a grid of spacing 0,5 deg in latitude and longitude covering the western North Atlantic or SWADE REGIONAL domain, The accuracy of the wind field was determined by comparing the measured winds in the SWADE array off the middle-Atlantic East Coast with the model

winds at the four closest grid points surrounding the buoy location, In the study of SWADE IOP-1 it was shown that the OWI wind fields provided sufficiently high spatial and temporal resolution to predict accurately the wave field during an intense mesoscale storm event (Graber et al. 1994; Cardone et al. 1995),

The ocean wave model used in the simulations described here is the third-generation WAM model, A very detailed description of the physical framework of the WAM model and numerous applications can be found in Komen et al. (1994). The version of the model implemented here is the Cycle-4 release of WAM, or WAM-4, in which the atmospheric boundary-layer is coupled to the wave model following Janssen (1991). In WAM-4, the evolution of the directional wave spectrum is specified on spherical coordinates defined by latitude and longitude and is determined from the integration of the energy balance equation (e. g., Graber, et al. 1995). Here we only consider deep water physics in the propagation and in the source terms. The wave-current option to include surface currents in this analysis was turned off, The three source terms consist of an empirical-based wind input function, the nonlinear energy transfer resulting from resonant wave-wave interactions, and the dissipation due to wave breaking or white-capping mechanism, Additional modifications of the source terms includes a quadratic dependency of the wind input on the ratio of friction velocity to wave celerity, and a dissipation which is proportional to the fourth power of the frequency. The wind input is given at standard height, usually 10 meters, and the surface stress is calculated internally within the wave model as a function of both wind speed at height and stage of wave development (i.e., a sea state-dependent drag coefficient).

WAM-4 was implemented on a nested grid system to represent the BASIN and REGIONAL SWADE domains. The BASIN grid covers the entire North and South Atlantic Oceans with a grid of 1 degree spacing, The BASIN grid hindcast with WAM-4 was run first and only once, using the ECMWF 6-hourly wind fields as input. This simulation was started five days prior to and continued throughout the simulation period (25 February to 9 March 1991) to provide overall spin up and continuous background wave conditions in the Atlantic ocean and provide directional spectra along the ocean boundaries of the REGIONAL model. The REGIONAL model covers the western North Atlantic with a grid spacing of 0.25 degree in latitude and longitude, Directional wave spectra are supplied from the BASIN grid to the eastern and southern boundaries to permit propagation of southern hemisphere swell into the SWADE region. The REGIONAL run was initially spun up with ECMWF winds over the five days prior to IOP-3 with input generated from the BASIN run. For the simulation period of IOP-3 we then used the OWI wind fields to predict the directional wave field and its parameters as well as the sea state dependent drag coefficient which multiplied with the square of the "effective" neutrally stable 10-m wind provides estimates of the surface wind stress, The direction of the wind stress was assumed to be in the direction of the wind. Output of these variables was available every hour over the entire SWADE REGIONAL domain.

4. KU-BAND MODEL FUNCTION STUDIES

Since the KU-band model function for friction velocity was developed using the FASINEX data with empirical techniques, it is important to conduct independent tests and evaluations of this model. Each daily data set was collected over approximately four hour or longer flight intervals. The radar cross section measurements were converted into friction velocity estimates using this model, at specific locations and times. These u^* estimates were then compared with the in-situ estimates discussed above. They were updated every hour and spanned the entire SWADE region of interest, ‘

A latitude and longitude grid with 0.25° resolution of friction velocity estimates was developed from the OWI/Miami dataset and technique. The area over which these friction velocity estimates are made spans the same regions of the ocean over which the aircraft scatterometer operated. The friction velocity maps are among the several variables (such as significant wave height, mean frequency, neutral stability wind, drag coefficient and wind direction) that were produced. Examples of this data set for March 7, 1991 are shown in Figures 1,2 and 3. Averages of four sequential hourly grids of the neutral stability wind speed, drag coefficient and friction velocity are shown in these figures. The 0.25° separations between adjacent values were interpolated to produce a finer spatial mesh. The strong spatial variability of the drag coefficient as seen in Figure 2 is a clear message that the neutral stability winds are not a sufficient indicator of the momentum flux at the air-sea interface,

The estimates of friction velocity inferred from the K-band scatterometer must be interpreted as 15 km and 2 minute averages, An example of these results is presented from the March 7 data set in Fig. 4. There are 19 useful flight paths on this day. A vertical line and a filled circle whose height is scaled to the u magnitude is placed at the individual average location of each path center. An interpolation program was used to create a mesh surface that estimates the u , throughout the observed region from these 19 points, Because of the intense spatial variability of u , this mesh surface obscures the view of some of the individual points. It should be kept in mind that this data set was collected over a time interval that extends to 4 hours, so that true simultaneity among all these points is not possible. The strong spatial variations apparent in this figure are seen to have much in common with the u plot from the Oceanweather /Miami estimates. These gradients occur in the radar data because the flight path locations were intentionally selected to cross the western edge of the Gulf Stream. The strong sea surface temperature variations in this region can be seen in the AVHRR thermal infrared color imagery displayed by Caruso, et al [1 994, see Appendix E].

Because of the appreciable time differences among the radar estimates, a more meaningful comparison was to match each acquisition time of the radar data with one of the times at which the OWI/Miami u maps were created (for example, Fig. 3). Each aircraft estimate of u can be compared with the closest u value (within 0.1° latitude and longitude, and within a one-half hour interval) from this in-situ model. The closer these values agree, the stronger the support for the validity of the FASINEX algorithm. However it should be kept in mind that the in-situ estimates of u are also subject to

some degree of error because of physical processes, the spatial resolution of the fundamental data upon which it is based and a possible time difference of 30 minutes,

Data from 8 days within this period was combined into a plot of scatterometer derived U , versus that produced by OWI/Miami. The comparison between the 2 different U estimates can be seen in Fig. 5. Two of the days in which radar data was collected could not be analyzed because of either unreliability or unavailability of the some data, The agreement is good. The vertical errorbars represent $\pm 15\%$. A possible cause of error may be the inability of this in-situ model to produce a reliable estimate of the drag coefficient and friction velocity when the sea spectrum of a strong mixture of both wind driven seas and incoming swell, whose propagating directions are at large oblique angles, This condition existed on February 28 and March 6,

On February 28, the sequence of flight paths connected to 3 different buoys which were widely separated by about 100 km. The relevant buoy locations for this days' flight are shown on a map in Figure 6, along with the flight tracks drawn with solid line segments. Buoys labeled "C", "E" and "CERC" served as destination points for the aircraft and critical data sources for the in-situ analysis described above. The directional wave spectra at each of these buoys, at the time of radar observations, show a combination of both wind driven seas (from the southwest) and westerly swell. The directional spectra are presented using polar wavenumber diagrams with contours to represent magnitudes and are overlaid in this map near the respective buoys. Each polar spectra is labeled with the time of data collection, the wind speed direction

(meteorological convention), the mean wave direction, "red", (oceanographic convention) and the direction of the spectral peak, "pal". A sample of the one-dimensional frequency spectrum for the CERC wave data is shown near the bottom of this map, next to the CERC directional spectra. It is obvious that on February 28, at the time of the radar measurement, the wave spectrum displayed strong bimodal properties. This complicated spectrum structure cannot be accurately included in the drag coefficient derivation. Any error in this estimated drag coefficient will induce an error in the u . estimate. A similar situation existed for the wave spectrum on March 6.

A quantitative assessment of this phenomena is seen in Fig, 7, in which we examine each days' results separately, The comparison between the u . estimates from the scatterometer and that of the in-situ analysis are plotted for each of the 8 days. Both February 28 and March 6 are different in that a majority of observations have the property that the two u . estimates differ by more than 25%. The other six days show a more consistent agreement between the scatterometer and in-situ estimates of u .. When these 6 other days data are all combined in a composite single plot (now without the Feb. 28 and Mar. 6 data) in Figure 8, the effective agreement is clearly seen to improve. The multiple correlation coefficient, R , is now 0.83, compared with $R = 0.72$ for the data set of Figure 8. The slope of the regression line, m , is now equal to 1.01 in Fig. 8 compared with $m = .83$ in Fig. 5. For about 90% of the data points in Fig, 8 the error bars ($\pm 15\%$ extensions) intersect the solid "equality" line. Another possible source of error may be the rapid spatial variability of u . in some locations with steep drops in magnitude, and the limited ability of the meteorological model to precisely position and

resolve these sharp spatial changes in these relatively small regions because of its larger spatial resolution.

Wind direction estimates also were compared. The azimuth scan measurement of the radar cross section by the scatterometer is acquired over a span of about 15 km across a flight track [Nghiem, et al, 1995]. Past experience with scatterometer studies indicate the azimuthal maximum is usually observed looking upwind. Using this indicator on each scatterometer circular scan, the wind direction was estimated, and it was then compared with the wind direction estimates by the OWI/Miami group. This comparison can be seen in Figure 9 for 7 days of data for all incidence angles: 20°, 30°, 40° and 50°, plotted separately. Numerous errors can be seen, mostly those due to a 180° ambiguity caused by an inversion of the NRCS maximum; it occurs when looking downwind instead of upwind. This is more prevalent at the 20° and 30° incidence angles than at 40° and 50°. Clearly, the 40° and 50° incidence angles have the fewest errors because at these incidence angles, the NRCS maximum occurs looking upwind in the large majority of situations. This has important implications for the NSCAT model function, in that the ability to estimate wind speed and direction depends on having a sufficiently larger upwind to downwind ratio. In most cases, no significant differences due to the polarization of the electromagnetic wave (vertical versus horizontal) were observed. The exception being for H-pol at 30°.

5. C-BAND MODEL FOR FRICTION VELOCITY

This model has the same general structure (a 3 term Fourier cosine series) as the well known Ku-band function [Wentz, et al, 1984]. The data used in this development was obtained from 9 of the 10 scatterometer flights. The experiment days of: Feb. 28, Mar, 1,2,4-9 were analyzed. C-Band NARCS data is available at incidence angles from 200 to 50° in 10° steps, and it has been processed to calculate the 3 Fourier coefficients (A_0, A_1, A_2) The coefficients, A_0 , A_1/A_0 and A_2/A_0 were plotted versus u^* , which was obtained from the simultaneous KU-band data used with the FASINEX algorithm.

The friction velocity, u_* , is estimated from the Ku-band A_0 measurement made over the same or closely adjacent flight segment. The incidence angle of the KU-band radar is selected independently of the C-band radar incidence angle. The only requirement is that it be at an angle at which there is an existing Ku-band algorithm between A_0 and u_* ; these are at: 20,30,40 and 50 degrees [Weissman, et al, 1994]

The results shown in Fig. 10 show the dependence of the C-band A_0 term on friction velocity. The 4 different incidence angles produce 4 distinguishable data sets that separate clearly in magnitude, and then in their dependence on friction velocity. The linear regression lines that were fit to each of the incidence angles' data have slopes that represent the exponent of a power law fit of A_0 to u_* at each angle. This slope gradually increases with the incidence angle: from 0.77 at 20° to 1.45 for 50°. These exponent magnitudes are all smaller than the values found for the Ku-band model function during FASINEX [Weissman, et al, 1994]. Generally speaking, this is in qualitative agreement

with the wind speed model function being developed for the ERS-I C-band scatterometer [Bentamy, et al, 1994].

The two other Fourier series coefficients, A_1 and A_2 , are observed here to have very different and distinctive properties in Fig. 11, The A_1/A_0 normalized term show generally small and highly random values at all the incidence angles. It appears to be too small (the average seems to be about 0,1) to have a critical role in the C-band scatterometer algorithm, The A_2/A_0 terms also shown in Fig 11, affects the upwind/crosswind ratio, and has an appreciable magnitude that increases with u , and with incidence angle. We see an increase in A_2/A_0 of a factor of approximately 5 between 20° and 50° incidence angles. However the dependence of A_2/A_0 on friction velocity is seen to have interesting properties once u^* reaches 0.4 m/s. For θ_i (incidence angle) = 30° , A_2/A_0 is seen to decrease with $u^* \geq 0.4$ m/s; for $\theta_i = 40^\circ$, A_2/A_0 levels off for $u^* \geq 0,4$, and for $\theta_i = 50^\circ$, A_2/A_0 continues to increase. This suggests that the electromagnetic scattering mechanism for 30° is different from that which is dominant at 50° ,

In order to use this AO function in the analysis of satellite or aircraft data where the incidence angle can lie anywhere between 20 and 50, the resolution of the functional dependence on incidence angle was improved using interpolation. The resulting $A(\theta)$ is plotted as a function of the 2 independent variables, in Fig. 12. This AO function can be used with the ERS-1 RCS data to infer the magnitude of u . Preliminary studies using this interpolated function have produced excellent results [Davidson, et al, 1995; Weissman, 1995]].

6. SUMMARY

The next logical step in evaluating the FASINEX KU-band model function has been performed. The friction velocity estimates derived from the NRSC measurements were compared with the best available spatial and temporally coincident data on a scale that had not previously possible. In every comparison data set the issue of the accuracy of the primary "standard" measurement must be clearly understood and explained. Generally speaking, in oceanographic experiments the most accurate physical measurements are associated with calibrated meteorological and oceanographic instruments on buoys, ships, stationary oceanographic towers or low flying aircraft. With respect to the type of resolution each of these could have, only the aircraft platform is restricted in terms of the time duration; the other platforms permit continuous monitoring of the desired quantities indefinitely. But, with respect to spatial resolution, the price of this high accuracy is to limit the measurements to a single point in space. During SWADE there were no low flying aircraft that were measuring the air-sea fluxes. Therefore there is no available technique that extends the same accuracy of "point" instruments to the large spatial areas traveled and observed by the scatterometer, in a sufficiently short time. The surface conditions; winds, waves and momentum flux, provided by the OWI techniques are the best compromise data set that is available with which to compare the scatterometer results. They represent a major innovation in estimating conditions at the air-sea interface over a wide area. However future extension of these studies are clearly indicated, to continue the development of this technique. Some of the assumptions used in this analysis should be critically re-examined. For example, the implications of neglecting the finite ocean depth in applying the WAM-4 model should be considered.

Also the possible wave-current interaction was not accounted for in these calculations, but it could be reconsidered in a future experiment in which detailed current data would be available. Another quantity that is of interest is the spatial variation of the air-sea temperature difference and the atmospheric stratification, with sufficiently high spatial resolution.

By choosing the 6 days during SWADE within which the combined meteorological and sea conditions were least complicated we were able to achieve excellent agreement between the two different friction velocity estimates, It is expected that this FASINEX KU-band model function will be applied to the satellite-based NASA Scatterometer measurements when they become available. These will provide estimates of the friction velocity at the sea surface on a global scale, However, the evaluation of its accuracy on this global scale becomes a more tenuous process than what was done here with the SWADE.data, because of the lack of surface instruments that can match the spatial and time scales of the satellite scatterometer swath, The evaluation of the satellite measurements and model function will require the observation of the regional, basin and global scale predictions (both meteorological and oceanographic) that are created from its data analysis. For oceanographic processes these will require long duration data sets (months and years). For meteorological studies and predictions, a rapid analysis using single satellite passes is usually the preferred situation.

The use of the difference between the upwind and downwind maximum in the azimuthal scan of the normalized radar cross section (NRCS) is the usual method by which the wind direction is estimated. Previous results with K.-band model function

studies have found that the magnitude of the NRCS looking upwind is larger than that looking downwind, on the average. [Wentz, et al, 1984; Weissman, et al, 1994]. This is equivalent to the AI term in the Fourier series model being a positive number. However, this difference decreases with incidence angle, and can display random fluctuations (and sign reversal) in response to the wide variety of effects induced by non-equilibrium seas. The results shown in Figure 9, where the radar derived estimates of wind direction are compared with the in-situ data, indicate some departure from the expectations for the 20° and 30° SWADE data, At these angles there is a higher probability (about 50% for 20°, and about 35% for 30°) that a radar-derived estimate of direction will be in error by 180°, because of the frequently observed inversion (negative AI), Results are much improved for the 40° and 50° observations; where the direction estimates are correct about 85% of the time.

The findings described above for the 20° analysis are not significantly different from what was determined in the data analysis of the FASINEX experiment. The FASINEX findings for A1/AO at this angle for V-pol and H-pol are that it is: “.. small, highly variable, and almost negligible. At 20° it is effectively zero”, The results for the 30° data in Fig. 9 do not identify which are the horizontal and vertical polarized data points, but the data records do indicate that the majority of the erroneous wind directions are associated with the V-pot measurements. These also agree with the FASINEX 30° results in which the AI /AO estimates tended to be lower (on average) for the V-pol case than H-pot, and that about 1/3 of these V-pol estimates produced negative AI's from the regression analysis in that study. It can be therefore be concluded that the results presented in Figure 9 are in substantial agreement with the Ku-band analysis conducted

with the FASINEX data.

The new results for a C-band model function for friction velocity are believed to be the first attempt to develop this type of algorithm using measured data, It also begins an era in which a Ku-band scatterometer is used to produce "in-situ" estimates of the surface friction velocity. The justification for this application is the successful comparison between the u , inferred from the KU-band scatterometer and that produced from the in-situ analysis by the OWI group, as presented in Section 4,

The properties of the AO vs u , power law approximations for each incidence angle shown in Figure 10 are reasonable in the sense that the magnitude of the exponent increases with incidence angle from 20° to 50° , and are smaller than the corresponding Ku-band V-pol cases, The next phase of evaluating this algorithm was to apply it to the data collected by the ERS-1 C-band satellite scatterometer in conjunction with supporting surface measurements. An opportunity arose to utilize this algorithm with ERS-1 passes near the coast of Norway during the NORCSEX '91 Calibration/Validation experiment for the newly launched instrument. In-situ measurements were provided by ship-base meteorological instruments, which included the friction velocity. [Davidson, et al, 1995]. Passes were analyzed whereby this C-band algorithm for AO, shown in Figure 12, was used to estimate the magnitude of u . These were then compared with the coincident shipboard measurements. The results show excellent agreement across the range of u , from 0.1 to 1 m/s, with difference less than about 10%. Additional studies are in progress based on more recent, but similar coordinated surface and satellite observations (e.g., NORCSEX '95). Also a complete model function is being formulated into a 3-

dimensional functional form that will enable it to be applied to larger scale ocean observations using wind retrieval algorithms to permit global scale studies of wind forcing and ocean circulation over monthly and annual intervals.

7. ACKNOWLEDGEMENTS

This research was sponsored by the Physical Oceanography Program of the National Aeronautics and Space Administration, Washington, D.C. The research performed by D. Weissman was sponsored through Grant No. NAGW-468 with Hofstra University, The research performed by R. McIntosh, S. Carson and J. Carswell was supported through a contract with the Remote Sensing Laboratory of the University of Massachusetts. The research performed by F. Li, S. Lou, S. Nghiem and G. Neumann was performed at the Jet Propulsion Laboratory, California Institute of Technology, under contract with NASA, The work of H. Graber was sponsored by the Office of Naval Research (ONR).

REFERENCES

- Anderson, R. J., 1993; A study of wind stress and heat flux over the open ocean by the inertial-dissipation method, *J. Phys. Oceanog.*, Vol. 23, October 1993, pp 2153-2161
- Barnier, B., M. Boukthir and J. Verron, 1991; Use of satellite scatterometer winds to force an ocean general circulation model, *J. Geophys. Res.*, Vol. 96, C1 2, pp 22,025-22,042, Dec. 15, 1991
- Barnier, B., J. Capella and J.J. O'Brien, 1994; "The use of satellite scatterometer winds to drive a primitive equation model of the Indian Ocean: the impact of band like sampling", *J. Geophys. Res.*, Vol. 99, No. C7, pp 14,187-14,196, July 15, 1994
- Bentamy, A., Y. Quilfen, P. Queffeulou and A. Cavanie, 1994; "Calibration of the ERS-1 Scatterometer C-band model", IFREMER/Brest Technical Report DRO/OS-94-01, January 1994
- Cardone, V. J., H. Graber, R. Jensen, S. Hasselmann, M. Caruso, 1995; "In search of the true surface wind field in SWADE IOP-1: ocean wave modeling perspective", *The Atmospheric and Ocean System*, In press
- Carson, S., R. McIntosh, A. Paylor, F. Li, G. Neumann, D. McLaughlin, 1992; "C-Eland measurement of radar backscatter from the ocean surface during SWADE", *IGARSS '92 Proceedings*, Vol. 1, p. 693, *IEEE Geoscience & Remote Sensing Symposium*, May 26-29, 1992
- Carswell, J. R., S. Carson, R. McIntosh, F. Li, G. Neumann, D. McLaughlin, J. Wilkerson, P. Black and S. Nghiem, 1994; "Airborne scatterometers: investigating ocean backscatter under low and high wind conditions", *Proc. IEEE*, Vol. 82, No. 12, December, 1994, pp 1835-1860
- Caruso, M. J., H.C. Graber, R.E. Jensen and M.A. Donelan, 1994a; *Surface Wave Dynamics Experiment*", Report 2, IOP-3, 25 Feb -9 March 1991, U.S. Army Corps of Engineers, Technical Report CERC-93-6, Report 2, March 1994, 294 pp.
- Caruso, M. J., K.A. Kelly, J. Metzger and H. Hurlburt, 1994b; *Comparison of ERS-1 Scatterometer and ECMWF wind forcing in the Kuroshio Extension Region*, American Geophysical Union Fall Meeting, Dec. 1994, San Francisco, CA.
- Davidson, K. L., D.E. Weissman, E. vanHalsema and R. Onstott, 1995; "Coastal applications of scatterometer wind algorithms", *OCEANS '95 Conference Proceedings*, San Diego, CA. (Oct. 9-12. 1995) ISBN No. 0-933957 -14-9 (IEEE Service Center)
- Donelan, M., F. Dobson, S. Smith, R. Anderson, 1993; "Dependence of sea surface roughness on wave development", *J. Phys. Oceanog.*, Vol 23, pp 2143-2149, September 1993

Freilich, M.H. and R.S. Dunbar, 1993 "A preliminary C-band scatterometer model function for the ERS-1 AMI instrument", First ERS-1 Symposium, Cannes, France, 4-6 November 1992, (Proceedings ESA SP-359, March 1993)

Freilich, M. H., 1995; Surface wind data from ERS-1 measurements, 1995 U.S. World Ocean Circulation Experiment Report, Implementation Report No. 7, Dept. of Oceanography, Texas A & M University, College Station, TX, July 1995, 56 pp

Graber, H. C., V. Cardone, R. Jensen, S. Hasselmann, H.L. Tolman and L. Cavaleri, 1994: The accuracy of wind field description, In: Komen et al., Dynamics and Modelling of Ocean Waves. Cambridge University Press, 285-293,

Graber, H. C., R.E. Jensen, V.J. Cardone, 1995: Sensitivity of wave model predictions on spatial and temporal resolution of the wind field, Proc. 4th Intl. Workshop Wave Hindcasting and Forecasting, Banff, Alberta, Canada

Geernaert, G.L. 1990;, "Bulk parameterizations for the wind stress and heat fluxes", in Surface Waves and Fluxes, Vol. 1- Current Theory, Edited by G.L. Geernaert and W.L. Plant, Kluwer Academic Publishers, 1990, Chapter 5

Janssen, P. A. E. M., 1991; Quasi-linear theory for wind-wave generation applied to wave forecasting. J. Phys. Oceanogr., 21, 1631-1642

Komen, G. J., L. Cavaleri, M. Donelan, K. Hasselmann, S. Hasselmann, and P. A. E. M. Janssen, 1994: Dynamics and Modelling of Ocean Waves .Cambridge University Press, 532pp.

Legler, D.M. and J.J. O'Brien, 1993; Comparison of ERS-1 Scatterometer and Florida State University tropical winds, Proceedings of Second ERS-1 Symposium, Hamburg, Germany, Oct. 11-14, 1993, (ESA SP-361)

Li, F, W, Large, W, Shaw, E.J. Walsh and K, Davidson 1989; "Ocean radar backscatter relationship with near-surface winds: a case study during FASINEX", J, Phys. Oceanogr., Vol. 19, pp 342-353, March 1989

McLaughlin, D. J., R.E. McIntosh, A. Pazmany, L. Hevizi and E. Boltmiew, 1991; "A C-band Scatterometer for remote sensing the air-sea interface", IEEE Trans. Geosci. Remote Sensing, Vol. 29, No. 2, March 1991, pp. 260-267

Nghiem, S. V., F. Li, S. Lou, G. Neumann, R. McIntosh, S. Carson, J. Carswell, E, Walsh, M. Donelan and W. Drennen, 1995; "Observations of radar backscatter at Ku and C bands in the presence of large waves during SWADE", IEEE Trans. Geosci. Remote Sensing, Vol. 33, No. 3, May 1995, pp 708-725.

Nordeng, T. E., 1991 On the wave age dependent drag coefficient and roughness length at sea, *J. Geophys. Res.*, Vol. 96, No. C4, pp 7167-7174, April 15, 1991

O'Brien, J. J., 1982; Scientific Opportunities Using Satellite Surface Wind Stress Measurements Over the Ocean, Report of the Satellite Surface Stress Working Group, June 1982, Nova University /N. Y.I.T. Press, Fort Lauderdale, FL., NASA Contract No, NAS5-26714

Smith, S. D., 1988; Coefficients for sea surface wind stress, heat flux, and wind profiles as a function of wind speed and temperature, *J. Geophys. Res.*, vol. 93, pp. 15,467-15,472, 1988.

Smith, S. D., R.J. Anderson, W. Oost, C. Kraan, N. Maat, J. DeCosmo, K. Katsaros, K. Davidson, K. Bumke, L. Hasse, H. Chadwick, 1992; "Sea surface wind stress and drag coefficients: the HEXOS results", *Boundary Layer Meteor.*, Vol 60, 1992, pp 109-142

Stage, S.A. and R.A. Weller, 1985; The Frontal Air-Sea Interaction Experiment (FASINEX); Part 1; Background and Objectives, *Bulletin of the American Meteorological Society*, 66 (12), 1511-1520, 1985

Stage, S.A. and R.A. Weller, 1986; The Frontal Air-Sea Interaction Experiment (FASINEX); Part II; Experiment Plan, *Bulletin of the American Meteorological Society*, 67 (1), 16-20, 1986

Weller, R. A., M.A. Donelan, M.G. Briscoe and N.E. Huang, 1991; Riding the Crest: A Tale of Two Wave Experiments, *Bull. Amer. Meteor. Soc.*, Vol. 72, No. 2, pp 163-183, February 1991

Weissman, D. E., 1994 "Studies of a C-Band Model Function for Friction Velocity Using Coincident, Simultaneous Ku-Band Scatterometer Measurements", *OCEANS '94 Conference Proceedings*, 13-16 Sept. 1994, Brest, France

Weissman, D. E., K. Davidson, R. Brown, C. Friehe, and F. Li, 1994; "The relationship between the microwave radar cross section and both wind speed and stress: model function studies using Frontal Air-Sea Interaction Experiment data" *J. Geophys. Res.*, Vol 99, C5, May 15, 1994

Weissman, D. E., 1995; "Scatterometer measurements of ocean surface stress from aircraft and from ERS-1", *OCEANS '95 Conference Proceedings*, San Diego, CA, (Oct. 9-12, 1995) ISBN No. 0-933957 -14-9 (IEEE Service Center)

Wentz, F. J., S. Peterherych and L.A. Thomas, 1984; A model function for ocean radar cross section at 14.6 GHz, *J. Geophys. Res.*, 89, pp 3689-3704

FIGURE CAPTIONS

Figure 1: Magnitude of the neutral stability wind speed estimated by Oceanweather, Inc./Univ. Miami methods, in the region where the airborne scatterometers operated, and spanning the same time interval. This is an average of 4 hourly estimates, on Mar 7. Resolution of 0.25° was interpolated to smaller grid.

Figure 2: Magnitude of the drag coefficient estimated by Oceanweather, Inc./Univ. Miami methods, in the region where the airborne scatterometers operated, and spanning the same time interval. This is an average of 4 hourly estimates, on Mar 7. Resolution of 0.25° was interpolated to smaller grid.

Figure 3: Magnitude of the friction velocity estimated by Oceanweather, Inc. /Univ. Miami methods, in the region where the airborne scatterometers operated, and spanning the same time interval. This is an average of 4 hourly estimates, on Mar 7. Resolution of 0.25° was interpolated to smaller grid.

Figure 4: Spatial variation of the friction velocity inferred from the K.-band scatterometer measurements on Mar, 7, during a 4 hour period, Each point is based on the average RCS over a 10-15 km flight segment. There are 19 data points used to create this mesh plot. Vertical lines indicate actual locations.

Figure 5. Results from 8 flight days; comparison from temporally and spatially coincident u. estimates between scatterometer estimates (ordinate) versus those from Oceanweather, Inc/Univ. Miami (abscissa). Solid line represents equality; dashed line represents the regression line. (m = slope of regression line, R = multiple correlation coefficient) The vertical error bars are $\pm 15\%$

Figure 6. A map indicating the principal flight tracks for the NASA C-130 aircraft and some buoy locations for the KU-radar data collected on Feb. 28, 1991. The buoy identifications are "C"r"E", "N", and "CERC". The solid lines display the aircraft ground track, and coincident directional wave spectra are overlaid.

Figure 7. Separate day presentations of the data in Fig. 5. The results are from 8 flight days; comparison from temporally and spatially coincident u. estimates between scatterometer estimates (ordinate) versus those from Oceanweather, Inc/Univ. Miami (abscissa). Solid line represents equality. The quality of agreement between the two different methods can be observed for individual days.

Figure 8. Results from 6 flight days, with data sets from Feb. 28 and March 6 omitted. This is a comparison for temporally and spatially coincident u. estimates; between scatterometer estimates (ordinate) versus those from Oceanweather, Inc/Univ. Miami (abscissa). Solid line represents equality; dashed line represents the regression line. (m = slope of regression line, R = multiple correlation coefficient) The vertical error bars are $\pm 15\%$

Figure 9: Comparison between the estimates of the wind direction, separated by incidence angle. Comparisons between scatterometer- derived wind direction (by selecting the direction of each azimuthal maximum) and estimates from Oceanweather, inc. /Univ. Miami group. Both horizontal and vertical polarizations.

Figure 10. The measured average C-band NRCS, AO, at each incidence angle (AO) vs. $u_{..}$. Data spans 9 flight days, duration of data collection at each incidence angle: 1 to 5 minutes. The magnitude of $u_{..}$ is estimated from the simultaneous measurement of AO from the K_u -band radar cross sections.

Figure 11: The corresponding C-band A1 and A2 terms for each data point in Fig. 10, normalized by AO, versus $u_{..}$. Separate plots for each incidence angle. Note the general increase in the magnitude of $A2/AO$ with incidence angle, and with $u_{..}$,

Figure 12: The graphical representation of the AO term, a function of both friction velocity and incidence angle, for the C-band model function, It is computed using an interpolation between the power law regression lines fit to the data of Fig. 10, to extend the results to incidence angles between the measured cases of 20,30,40 and 50 degrees.

Mar 7- Neutral Winds, Averaging Time=21 :00-24:00

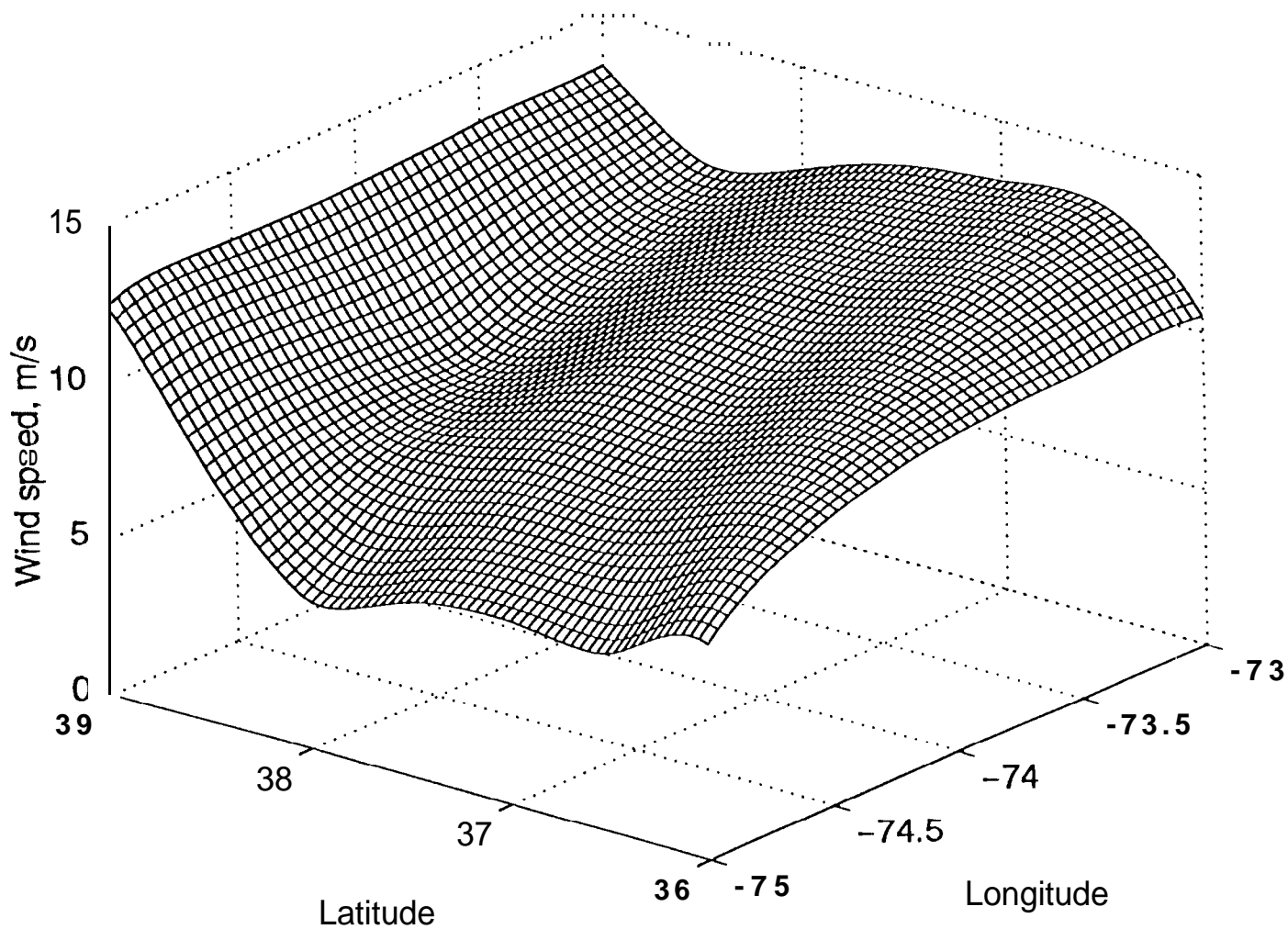


Figure 1: Magnitude of the neutral stability wind speed estimated by Oceanweather, inc. /Univ. Miami methods, in the region where the airborne scatterometers operated, and spanning the same time interval. This is an average of 4 hourly estimates, on Mar 7. Resolution of 0,25° was interpolated to smaller grid.

Mar 7- Drag Coefficient, Cd, Averaging Time=21 :00-24:00

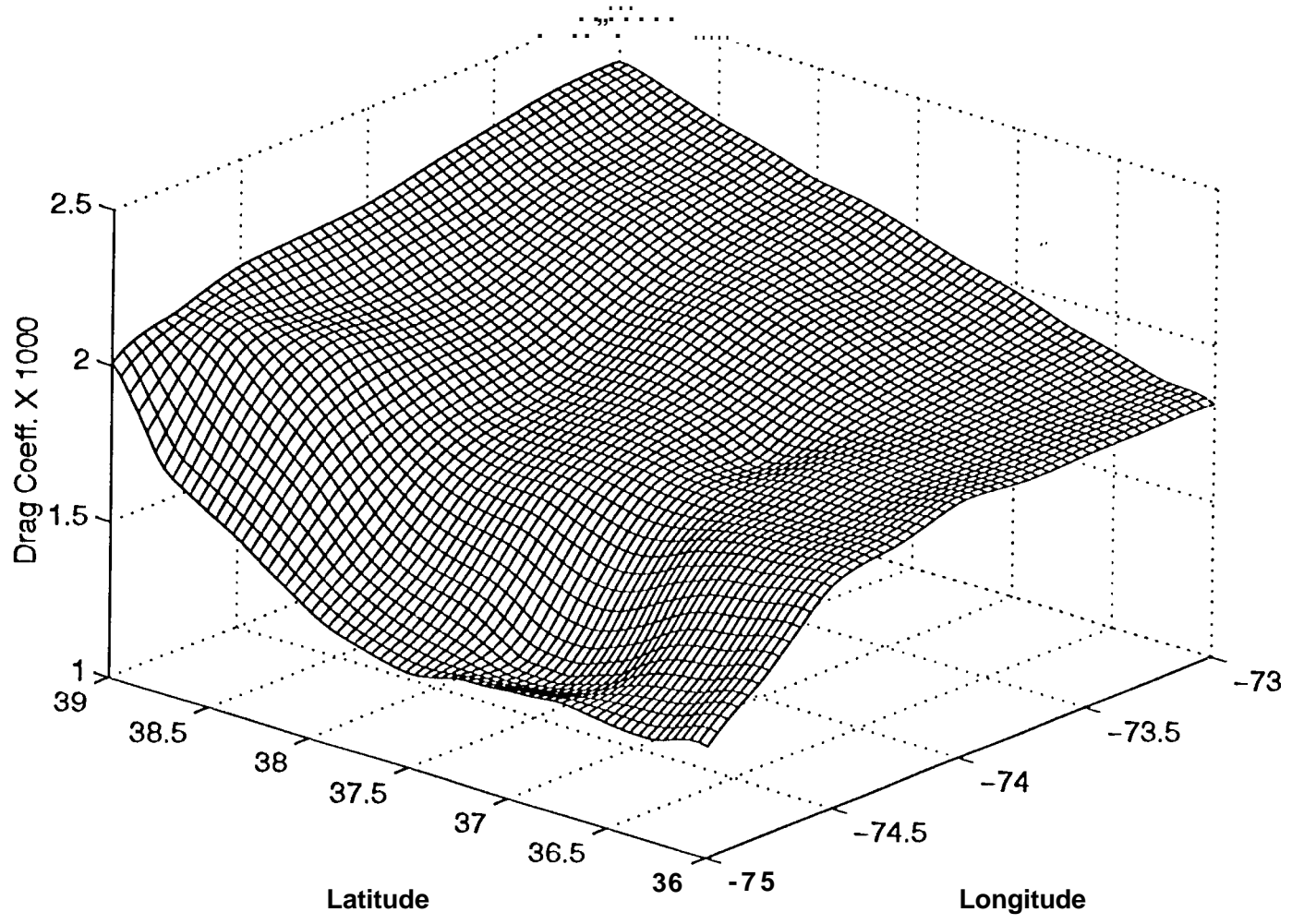


Figure 2: Magnitude of the drag coefficient estimated by Oceanweather, Inc./Univ. Miami methods, in the region where the airborne scatterometers operated, and spanning the same time interval. This is an average of 4 hourly estimates, on Mar 7. Resolution of 0.25° was interpolated to smaller grid.

Mar 7- Friction Velocity, u' , Averaging Time=21 :00-24:00

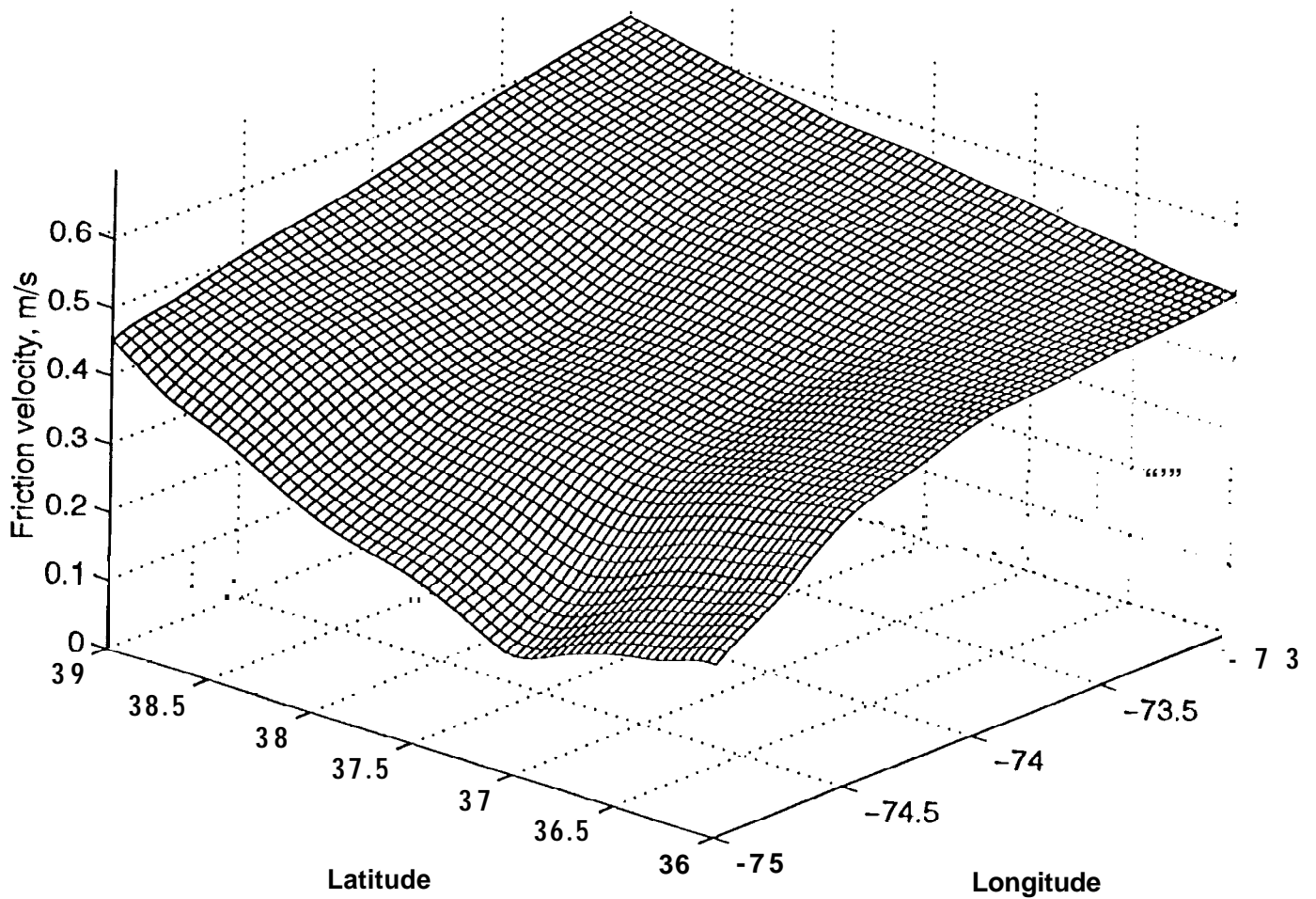


Figure 3: Magnitude of the friction velocity estimated by Oceanweather, Inc./Univ. Miami methods, in the region where the airborne scatterometers operated, and spanning the same time interval, This is an average of 4 hourly estimates, on Mar 7. Resolution of 0.25° was interpolated to smaller grid,

Mar 7- Friction Velocity interpolated betw. scat. locations (4 hour)

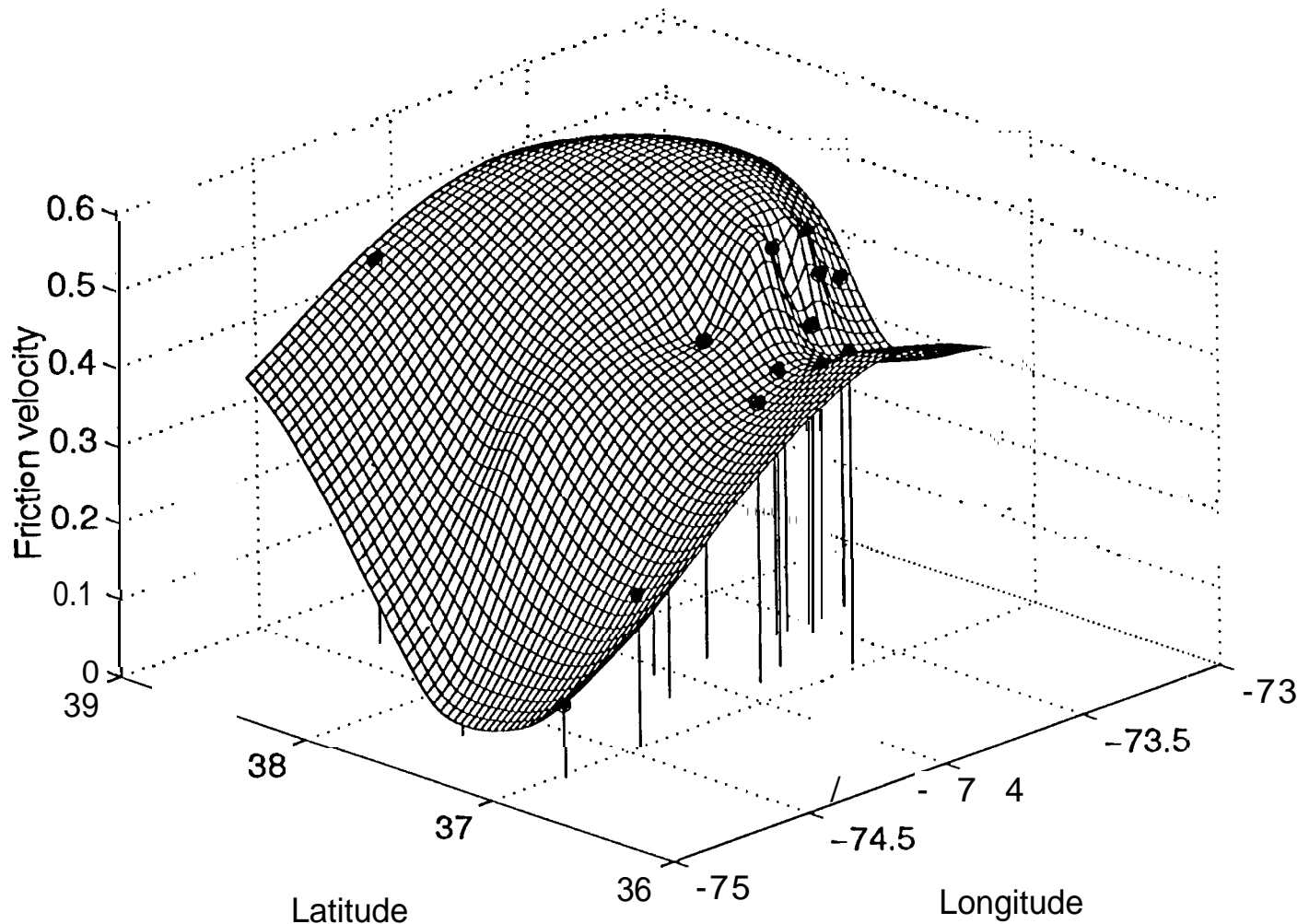


Figure 4: Spatial variation of the friction velocity inferred from the KU-band scatterometer measurements on Mar, 7, during a 4 hour period. Each point is based on the average RCS over a 10-15 km flight segment. There are 19 data points used to create this mesh plot. Vertical lines indicate actual locations,

Comparison of u^* from Scatterometer NRCS with in-situ estimates

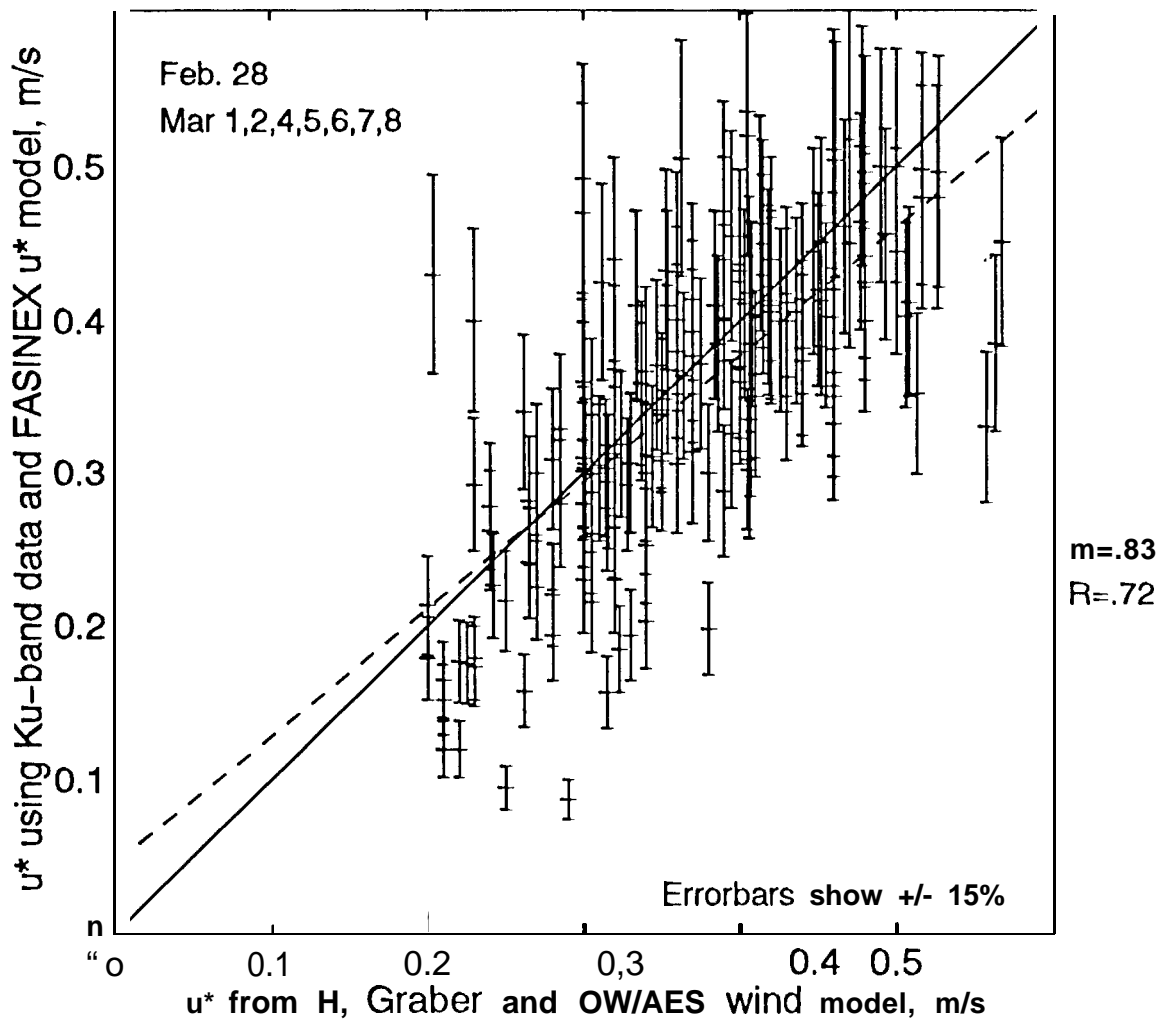


Figure 5. Results from 8 flight days; comparison from temporally and spatially coincident u^* estimates between scatterometer estimates (ordinate) versus those from Oceanweather, Inc/Univ. Miami (abscissa), Solid line represents equality; dashed line represents the regression line. (m = slope of regression line, R = multiple correlation coefficient) The vertical error bars are $\pm 15\%$

Buoy Locations (N, E,C and CERC) and Scatterometer Flight Tracks for Feb. 28

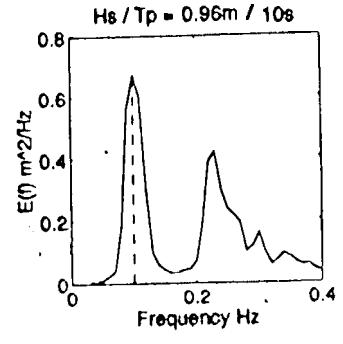
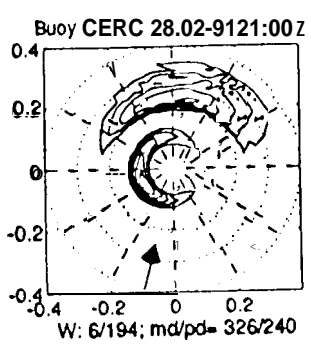
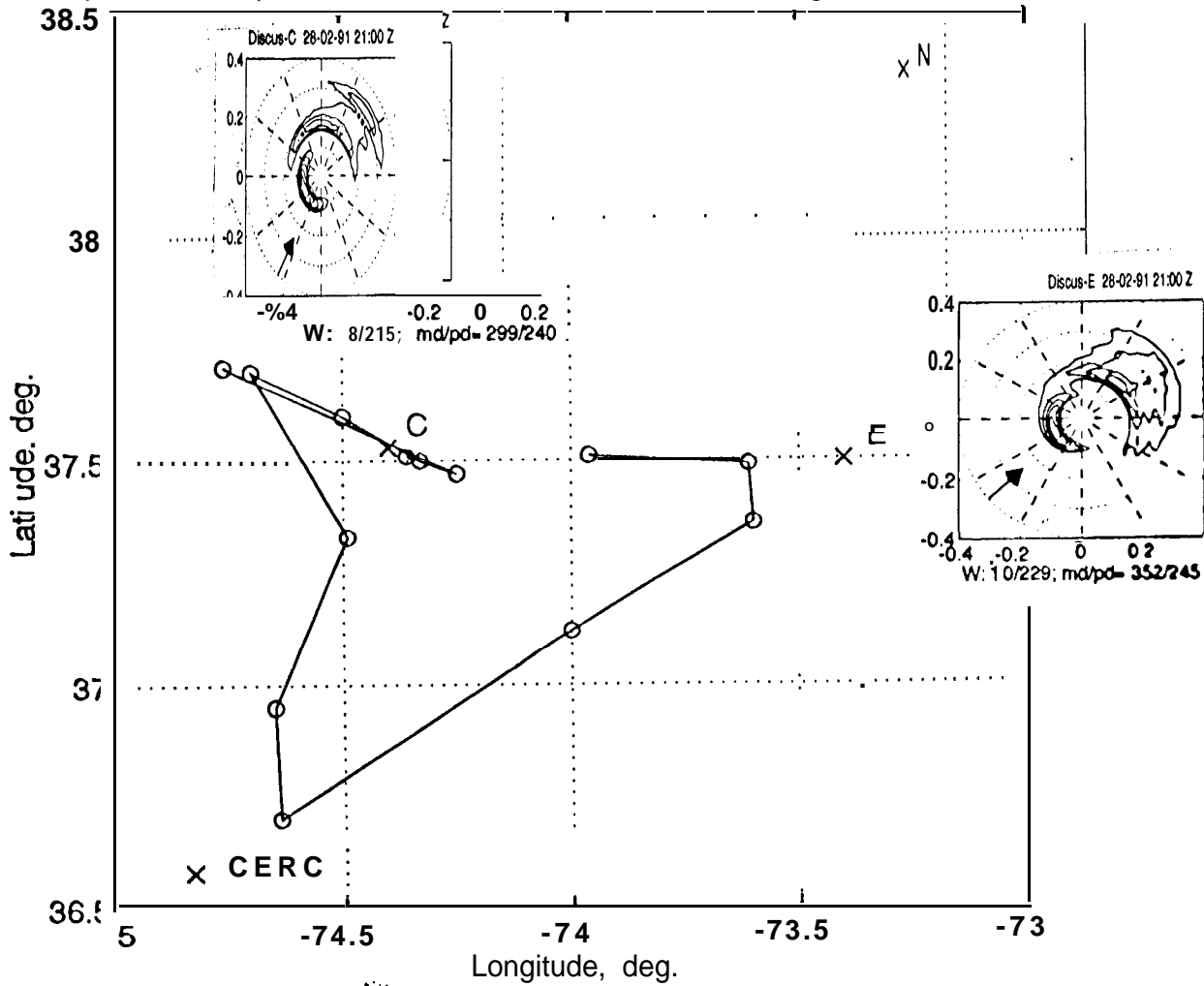


Figure 6. A map indicating the principal flight tracks for the NASA C-130 aircraft and some buoy locations for the KU-radar data collected on Feb. 28, 1991. The buoy identifications are "C", "E", "N", and "CERC". The solid lines display the aircraft ground track, and coincident directional wave spectra are overlaid.

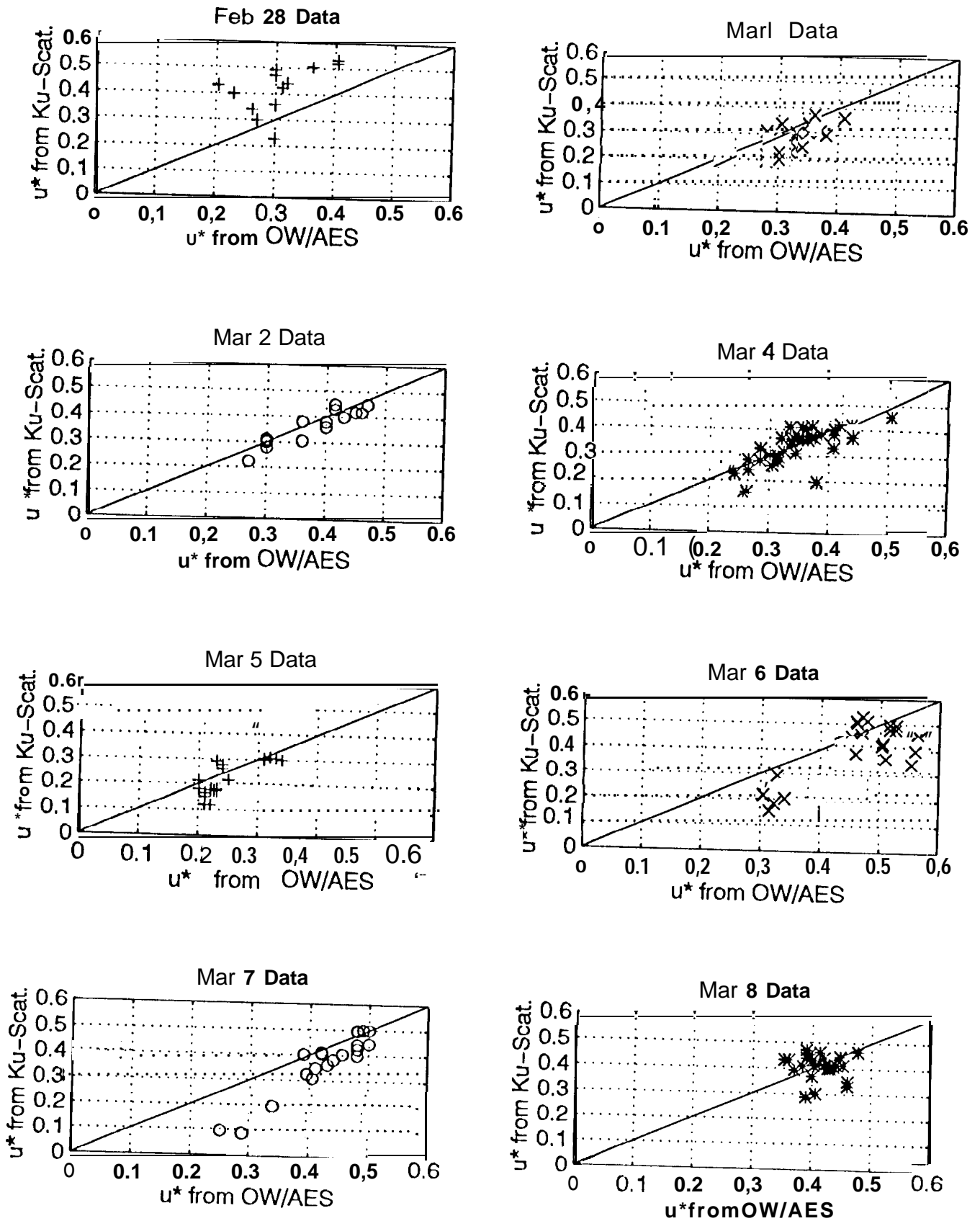


Figure 7. Separate day presentations of the data in Fig. 5. The results are from 8 flight days; comparison from temporally and spatially coincident u^* estimates between scatterometer estimates (ordinate) versus those from Oceanweather, Inc/Univ. Miami (abscissa). Solid line represents equality. The quality of agreement between the two different methods can be observed for individual days.

Comparison of u^* from Scatterometer NRCS with in-situ estimates

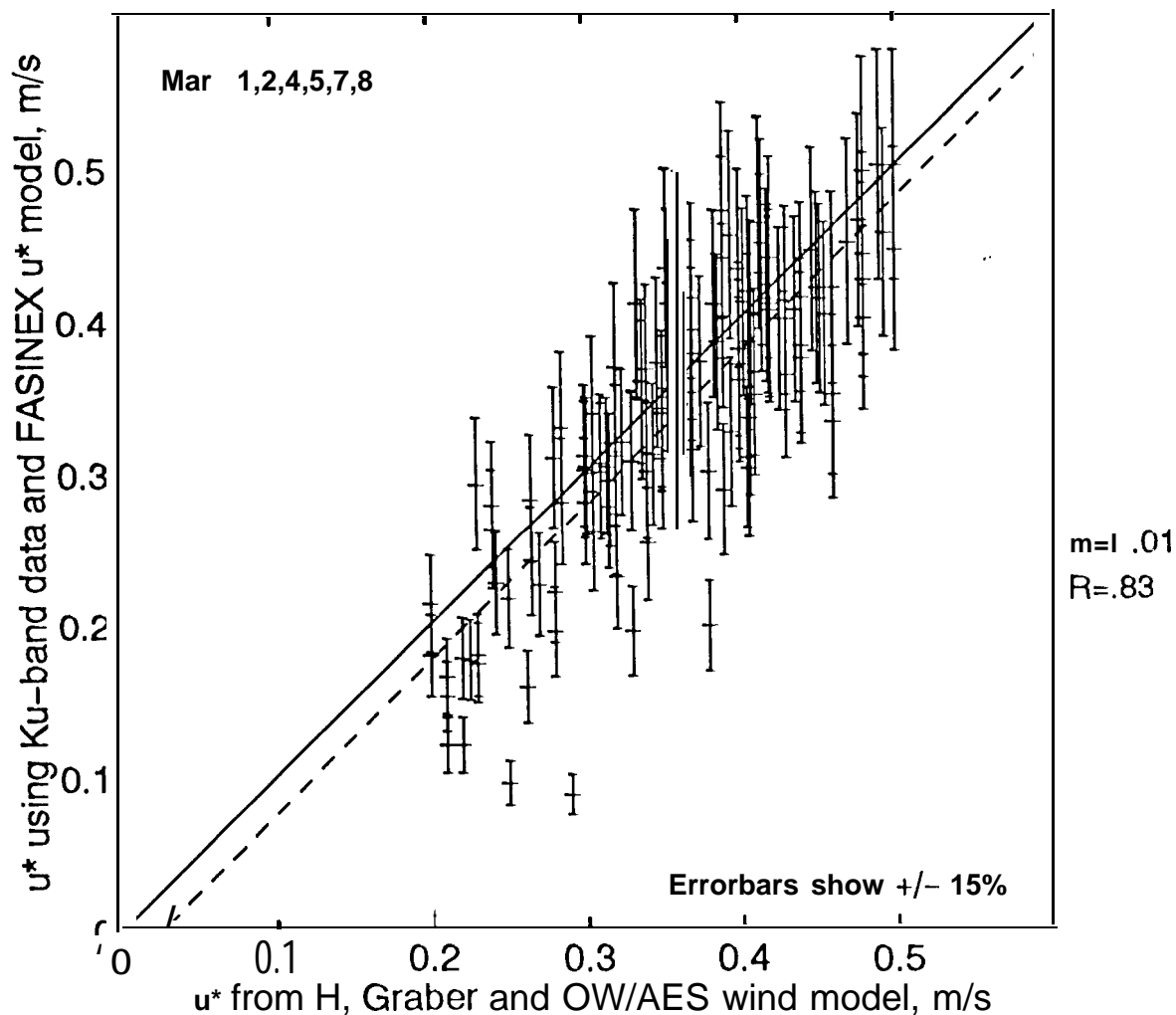


Figure 8. Results from 6 flight days, with data sets from Feb. 28 and March 6 omitted. This is a comparison for temporally and spatially coincident u^* estimates; between scatterometer estimates (ordinate) versus those from Oceanweather, Inc/Univ. Miami (abscissa). Solid line represents equality; dashed line represents the regression line. (m = slope of regression line, R = multiple correlation coefficient)

The vertical error bars are $\pm 15\%$

All 7 Days of Directional Data, Separated into 20,30,40 and 50 deg, incidence.

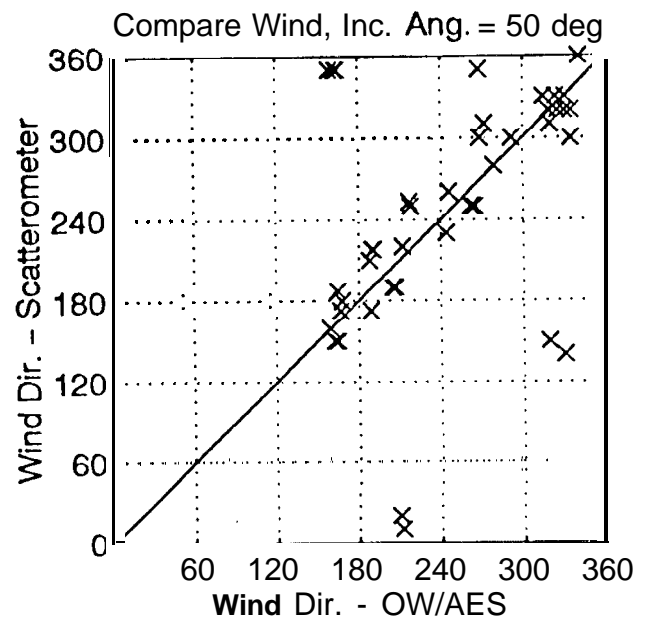
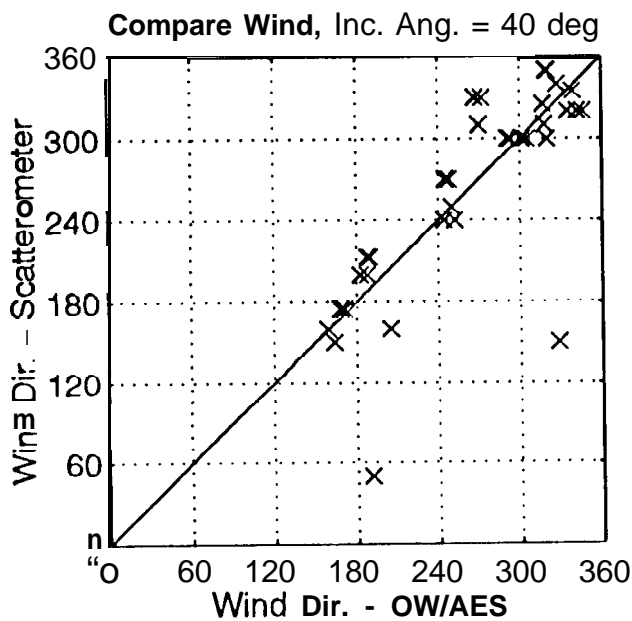
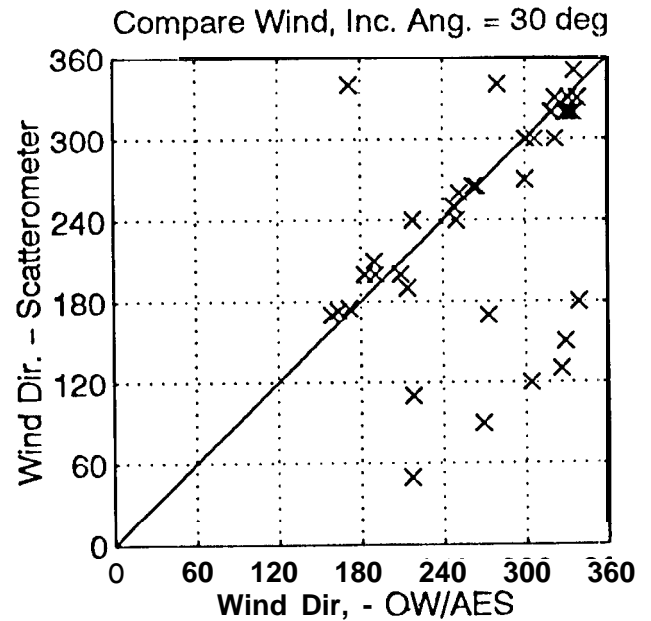
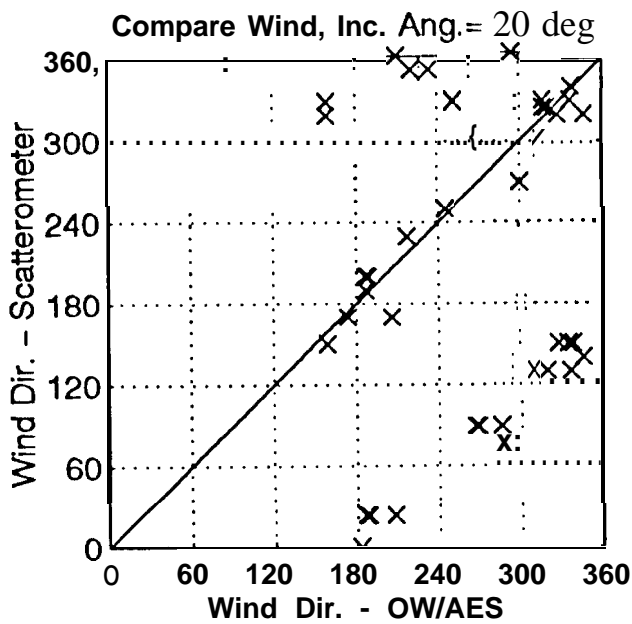


Figure 9: Comparison between the estimates of the wind direction, separated by incidence angle. Comparisons between scatterometer-derived wind direction (by selecting the direction of each azimuthal maximum) and estimates from Oceanweather, Inc./Univ. Miami group. Both horizontal and vertical polarizations.

C-Band Avg RCS - AO, Feb 28, Mar 1,2,4-9

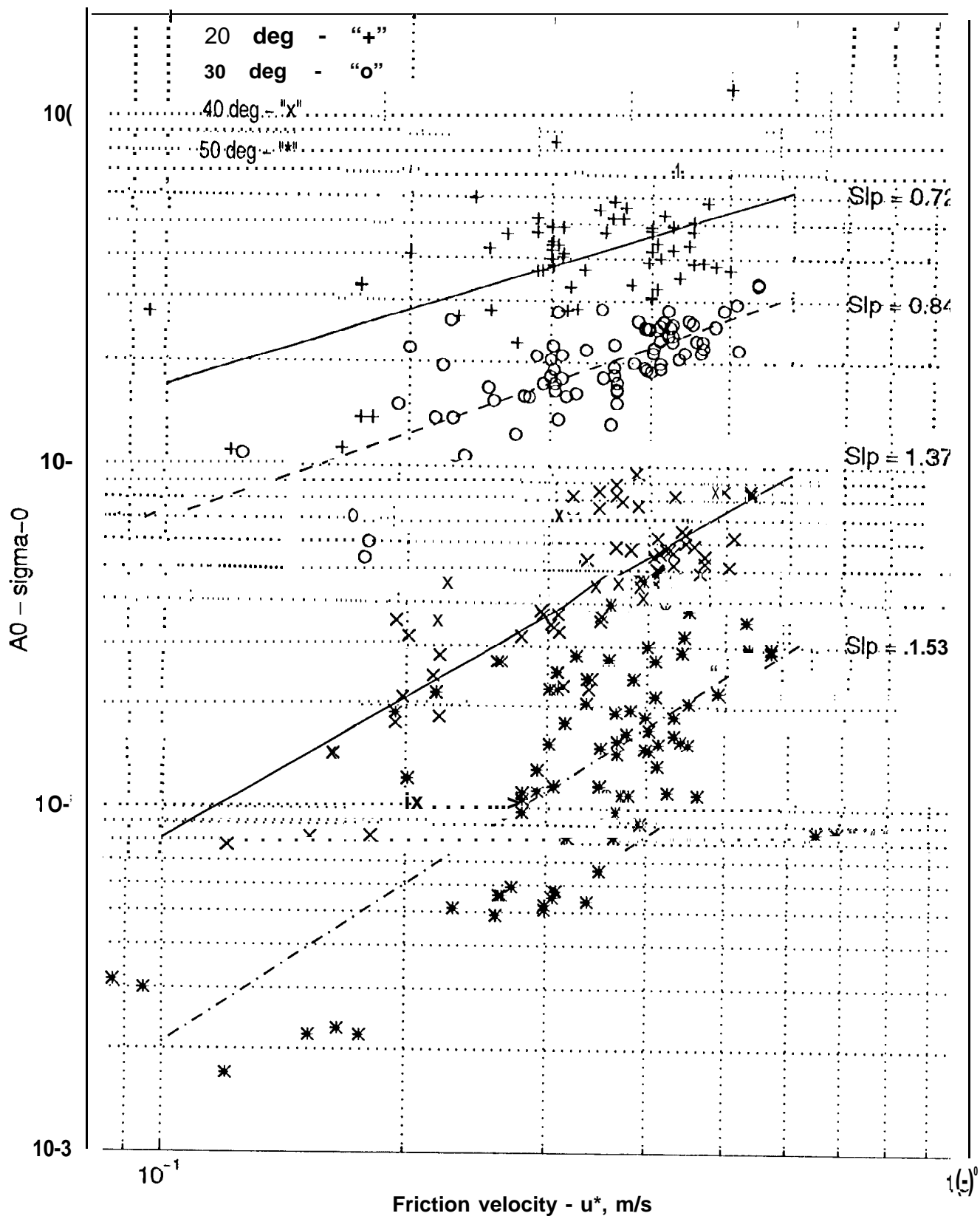


Figure 10. The measured average C-band NRCS, AO, at each incidence angle (AO) vs. u^* . Data spans 9 flight days, duration of data collection at each incidence angle: 1 to 5 minutes. The magnitude of u^* is estimated from the simultaneous measurement of AO from the Ku-band radar cross sections.

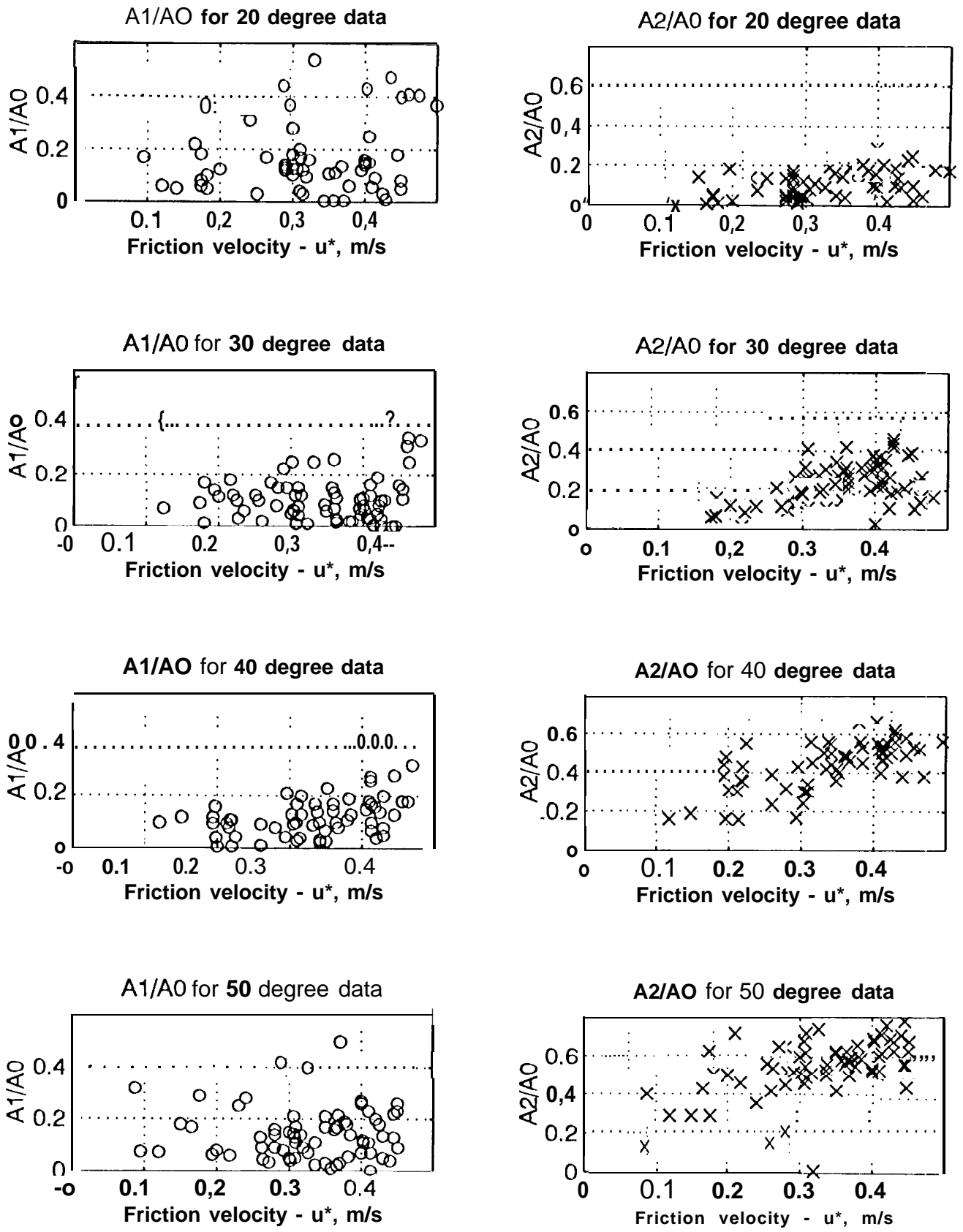


Figure 11: The corresponding C-band A1 and A2 terms for each data point in Fig. 10, normalized by A0, versus u . Separate plots for each incidence angle. Note the general increase in the magnitude of A2/A0 with incidence angle, and with u .

C-Band Model Function - Interpolated from Regression Curves

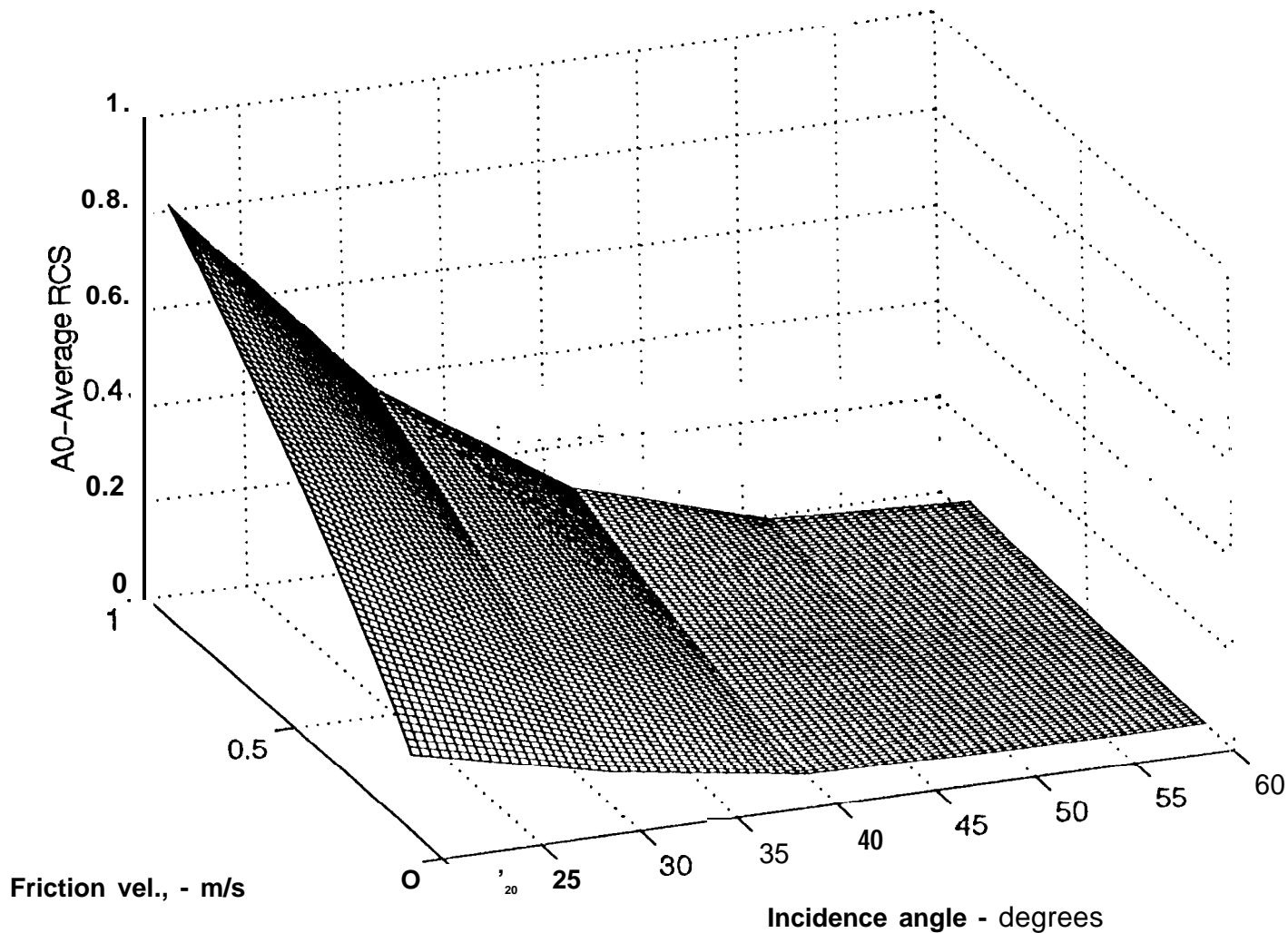


Figure 12: The graphical representation of the AO term, a function of both friction velocity and incidence angle, for the C-band model function, it is computed using an interpolation between the power law regression lines fit to the data of Fig. 10, to extend the results to incidence angles between the measured cases of 20,30,40 and 50 degrees.